First-principles study of diffusion behaviors of Cs and I in Cr coating*

Shuying Lin,[1] Xiaojing Li,[1] Linbing Jiang,[1] Xijun Wu,[2] Huiqin Yin,[1] Yu Ma,[1,†] and Wenguan Liu[1,‡]

[1]Sino-French Institute of Nuclear Engineering and Technology, Sun Yat-Sen University, Zhuhai, 519082, China
[2]School of Nuclear Science and Technology, University of South China, Hengyang, 421001, China

Cs and I can migrate through the fuel-cladding interface and accelerate the cladding corrosion process induced by the Fuel Cladding Chemical Interaction. Cr coating is an important candidate in mitigating this chemical interaction. First-principles calculations were employed to investigate the diffusion behaviors of Cs and I in Cr bulk and Cr grain boundary, aiming to reveal the microscopic mechanisms for mitigating the interaction at fuel-cladding interface. The interactions between these two fission products and Cr coating were systematically studied, and the temperature-dependent diffusion coefficients of Cs and I in Cr were obtained using Bocquet's oversized solute atoms model and Le Claire's nine-frequency model, respectively. The results show that the migration barriers of Cs and I are significantly lower compared to that of Cr, and the diffusion coefficients of Cs and I are both more than 3 orders of magnitude larger than Cr self-diffusion coefficient within the temperature range of Generation IV fast reactors (below 1000 K), which shows the strong penetration ability of Cs and I. Meanwhile, Cs and I are more likely to diffuse along the grain boundary because of the generally low migration barriers, indicating that grain boundary serves as a fast diffusion channel for Cs and I.

Keywords: First-principles calculation, Fuel Cladding Chemical Interaction, Cr coating, Fission product, Diffusion, Grain boundary

I. INTRODUCTION

Fuel Cladding Chemical Interaction (FCCI) is considered as one of the major factors limiting the lifetime of fuel pins in fast reactors, especially for oxide fuel pins with stainless steel cladding [1], as severe oxidative corrosions can occur on the interface of the fuel and the inner wall of the cladding. Some fission products, migrating through the fuel-cladding interface, can accelerate the FCCI-induced cladding corrosion process, and the main fission products involved are volatile Cs and I [1, 2] considering their production yield and penetrating depth. As the cladding attack rate depends on diffusion of reactants at cladding surface, the diffusion of Cs and I in fuel pins is a key factor in FCCI-induced corrosion problem.

Due to the complex and multiscale coupled physical and chemical mechanisms of FCCI, current research mainly focuses on exploring materials that can mitigate FCCI through experimental studies, and a coating of buffer-getter materials on the cladding inner surface is considered as an effective method [1]. The buffer-getter materials including V, Nb, Cr, Zr, U, Ti and certain rare earth metals can reduce oxidation of the cladding due to their high affinity for oxygen [1]. Specifically, Cr coating features a high melting point, superior oxidative corrosion resistance [3, 4], good crack resistance [5–7], and mature preparation processes [8–10], making it an important candidate in mitigating FCCI, but the underlying micro-mechanisms remain unknown. First-principles density functional theory (DFT) is recognized as a powerful tool to reveal the micro-mechanisms, especially from the perspective of elemental diffusion behaviors when coupled with harmonic transition state theory [11], as proved by numerous previous works for impurity diffusion including its consequent effects in Ni [11–16], Fe [17–24], Al [25–27], SiC [28], etc. Recently, Yang et al. have carried out first-principles calculations of lanthanides diffusion in Cr and α-Fe to identify the FCCI-mitigating mechanisms for metallic fuel and ferritic/martensitic steel cladding system [22]. According to our knowledge, there are still few investigations of FCCI-involved elements for oxide fuels, in which Cs and I dominate. Besides, further investigation is warranted to comprehensively understand the effects of Cr coating on the cladding inner surface functions in mitigating FCCI for oxides fuel pin systems.

In this work, first-principles method was employed to investigate the diffusion behaviors of important fission products (Cs and I) in BCC Cr coating. Cs and I are so large in the Cr matrix that the diffusion mechanism by interstitial atoms [29–33] was deemed unrealistic. Instead, vacancy-mediated mechanism is the main mode of diffusion for impurity atoms of large atomic size [34], such as Cs and I. Section 2 lays out the vacancy-mediated diffusion models and details of the first-principles calculations. The methodology to determine the inputs for diffusion models is also presented. Section 3 discusses the interactions between impurity atoms and the surrounding Cr atoms or vacancies. Diffusion coefficients of Cs and I in BCC Cr were obtained by applying the diffusion model, and possible diffusion paths of Cs and I at grain boundary (GB) were predicted based on results of migration barriers between different sites.

* This work was supported by National Natural Science Foundation of China (No. 12375282) and the Project of Key Laboratory of Computational Physical Sciences (Fudan University), Ministry of Education.
† Corresponding author, mayu9@mail.sysu.edu.cn
‡ Corresponding author, liuwg7@mail.sysu.edu.cn

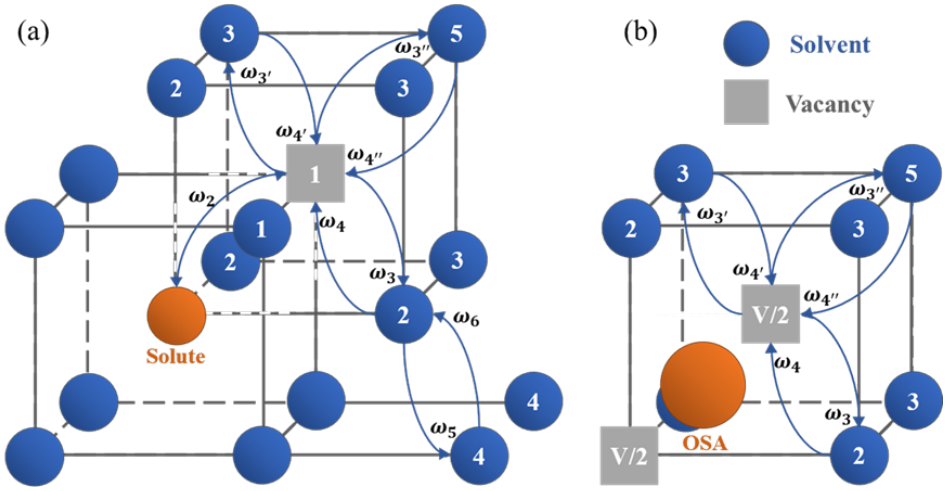

Fig. 1. (Color online) Illustration of diffusion models: (a) Le Claire's model [35–37]; (b) OSA model [21].

II. COMPUTATIONAL METHODS

A. Diffusion models for vacancy-mediated solutes

In this section, two diffusion models for determination of impurity diffusion coefficients were introduced, namely Le Claire's nine-frequency model [35–37] (referred to as Le Claire's model below) and the oversized solute-atom (OSA) model [21]. As shown in Fig. 1, impurity atoms and matrix atoms are represented by orange and blue spheres, respectively, and vacancies by gray squares. The numbers on the atoms and vacancies indicate their positions as the nearest neighbors (nn) to the impurity atom. The corresponding jump frequencies for different atom-vacancy exchange processes are also labeled in Fig. 1. The main difference between the two diffusion models lies in the configuration formed by the impurity atom and its 1nn vacancy, which will be described in details in the following.

According to the Le Claire's model [35–37], the self-diffusion coefficient ($D_{self-diff}$) and the solute diffusion coefficient (D_{solute}) in BCC lattice can be obtained by:

$$D_{self-diff} = a^2\omega_0 f_0 C_V, \tag{1}$$

$$D_{solute} = a^2\omega_2 f_x C_V exp(\frac{E_1^b}{k_B T}), \tag{2}$$

with a the lattice parameter, E_1^b the vacancy-solute binding energy when the vacancy is located on the 1nn site of the solute, k_B the Boltzmann constant and T the temperature in K. f_0 is the correlation factor for self-diffusion, and is a constant equal to 0.727 for diffusion in BCC crystals. The correlation factor for solute diffusion f_x can be expressed as [35–37]:

$$f_x = \frac{3\omega_3 + 3\omega_{3'} + \omega_{3''} - \frac{\omega_3\omega_4}{\omega_4 + F\omega_5} - \frac{2\omega_{3'}\omega_{4'}}{\omega_{4'} + 3F\omega_0} - \frac{\omega_{3''}\omega_{4''}}{\omega_{4''} + 7F\omega_0}}{2\omega_2 + 3\omega_3 + 3 + \omega_{3''} - \frac{\omega_3\omega_4}{\omega_4 + F\omega_5} - \frac{2\omega_{3'}\omega_{4'}}{\omega_{4'} + 3F\omega_0} - \frac{\omega_{3''}\omega_{4''}}{\omega_{4''} + 7F\omega_0}}, \tag{3}$$

where $F = 0.512$. This expression applies to the case where the impurity atom is close in size to the matrix atom, with approximation $\omega_6 = \omega_0$. Based on the transition-state theory [35], the average atomic jump frequency ω_i can be written with respect to the migration energy (E_i^m) as:

$$\omega_i = \nu_i exp(-\frac{E_i^m}{k_B T}), \tag{4}$$

in which ν_i and E_i^m are the attempt frequency and corresponding migration barrier for jump i, respectively. ν_i is defined as $\nu_i = \prod_{j=1}^{3N-3}\nu_j^I / \prod_{j=1}^{3N-4}\nu_j^T$, in which ν_j^I is normal vibration frequencies of the initial state (I) of migration, and ν_j^T is the nonimaginary normal frequencies of the transition state (T). The vacancy concentration at equilibrium at temperature T is given by $C_V = exp(-\frac{E_v^f}{k_B T})exp(\frac{S_v^f}{k_B})$, with the vacancy formation energy $E_v^f = E^I - (N-1)E^B/N$ and the vacancy formation entropy $S_v^f = k_B[\sum_{j=1}^{3N-3} ln(\frac{k_B T}{h\nu_j^I}) - \frac{N-1}{N}\sum_{j=1}^{3N} ln(\frac{k_B T}{h\nu_j^B})]$, in

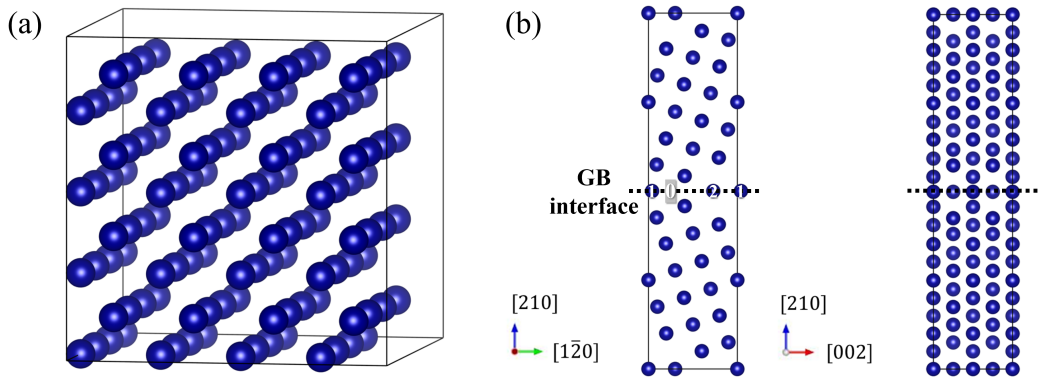

Fig. 2. (Color online) Illustration of simulation models for Cr matrix and GB. (a) 4 × 4 × 4 supercell containing 128 atoms representing Cr matrix; (b) Cr Σ5(210) GB with 76 atoms, where the atomic sites at GB interface are labeled by the numbers (0 for interstitial site, 1 & 2 for substitutional sites).

which E^I and E^B are the corresponding energy of the initial state structure and the bulk structure containing $N-1$ and N atoms, respectively, and ν_j^B is normal vibration frequencies of the bulk structure (B).

The Le Claire's model is the commonly used diffusion model which describes well the diffusion of substitutional solutes. Nevertheless, due to the strong attraction of the OSA to the vacancy (as illustrated in Fig. 1 (b)), the diffusion of OSA cannot be described by Le Claire's model. Bocquet et al. proposed a diffusion model applicable to OSA, i.e. the OSA model, and the expression for OSA diffusion coefficient is given by [21]:

$$D_{OSA} = \frac{\lambda^2}{12}\Gamma_{MJ} f, \tag{5}$$

where λ is the distance between the vacancy and its nearest atom, i.e. $\lambda = \sqrt{3}a/2$ in BCC crystals, Γ_{MJ} is the frequency attached to a macrojump (MJ), and f is the correlation factor. A macrojump is formed by 2 elementary displacements: the OSA located on a substitutional site (S) is pushed onto a transitional site (T), i.e., S → T, and then moved onto a S site from T site (T → S). In this way the frequency attached to a MJ is defined as: $\Gamma_{MJ} = \Gamma_{ST}\Gamma_{TS}/(\Gamma_{ST}+\Gamma_{TS})$ with $\Gamma_{ST} = 8C_V[3\omega_4 exp(\frac{E_2^b}{k_BT}) + 3\omega_{4'} exp(\frac{E_3^b}{k_BT}) + \omega_{4''} exp(\frac{E_5^b}{k_BT})]$ and $\Gamma_{TS} = 2\times(3\omega_3 + 3\omega_{3'} + \omega_{3''})$. E_i^b is the binding energy between the solute and its i^{th} nn vacancy (positive value for attraction, and vice versa), and can be calculated by:

$$E_i^b = E^V + E^S - E^I - E^B. \tag{6}$$

The terms on the right side of the equation represent the energies of different configurations, and the numbers of Cr atoms, vacancies, and impurity atoms in each configuration are (127, 1, 0), (127, 0, 1), (126, 1, 1), and (128, 0, 0), respectively. The correlation factor f for OSA diffusing in BCC crystals equals to $1+Q^{BCC}$, in which Q^{BCC} is the average cosine between a T → S jump vector and the next S → T jump in the BCC lattice. Bocquet et al. obtained the exact formula of Q^{BCC} by a double Laplace and Fourier transform of the transport equation for the vacancy. But for simplification, here we applied the formula with the "one-shot" approximation [21]:

$$Q_{1shot}^{BCC} = -\frac{1}{3\omega_3 + 3\omega_{3'} + \omega_{3''}} \times \left(\frac{4\omega_3\omega_4}{4\omega_4 + 4\omega_5} + \frac{4\omega_{3'}\omega_{4'}}{2\omega_{4'} + 6\omega_0} + \frac{\omega_{3''}\omega_{4''}}{\omega_{4''} + 7F\omega_0}\right). \tag{7}$$

The hypothesis of the "one-shot" approximation is that, after the dissociation of the OSA and its nearby vacancy, only one jump is needed for the vacancy to return close to the OSA. It is proved available when the vacancy-solute interaction is very strong at 1nn, which is exactly the case of OSA diffusion.

Our preliminary calculation show that Cs combines with its 1nn vacancy and forms a configuration of "V/2 + Cs + V/2" (V for vacancy), corresponding to Fig. 1(b). In contrast, I does not exhibit strong attraction to 1nn V, corresponding to Fig. 1(a). According to the applying conditions for different diffusion models, the OSA model is used for the calculation of Cs diffusion coefficients, and the Le Claire model is used for I in this study.

B. First-principles calculation

To investigate the diffusion behaviors of Cs and I in BCC Cr coating, the density functional theory (DFT) calculations are performed with the Vienna ab initio simulation package (VASP) [39–41] using the projector augmented wave (PAW) [42] pseudopotentials and Perdew-Burke-Ernzerhof (PBE) [43] parametrization. Razumovskiy et al. found that disordered local-moment calculations for pure Cr in the paramagnetic state will reduce to a nonmagnetic solution [44]. A $4 \times 4 \times 4$ supercell containing 128 atoms was adopted for the simulation of Cr matrix, and the $\Sigma5(210)$ GB supercell consisting of 76 sites for simulation at Cr GB, as shown in Fig. 2. The Brillouin area was sampled with the $4 \times 4 \times 4$ and $5 \times 5 \times 1$ k-point meshes for Cr matrix and GB, respectively. The total energy and force convergence criteria were set to 1.0×10^{-5} eV and 0.01 eV/Å, respectively, with a cutoff energy of 400 eV. All transition states and migration barriers were obtained by applying the climbing image Nudged Elastic Band (cNEB) method, using 3 intermediate images. To determine the diffusion coefficients in Cr matrix, phonon calculations were also performed considering only the vibrational modes of the migrating atoms [22, 45–48]. For both the search of transition states and phonon calculations, the force convergence criterion was reset to 0.001 eV/Å, as the results are highly sensitive to this parameter.

III. RESULTS AND DISCUSSION

A. Impurity diffusion in Cr matrix

1. Atomic structure and electron distribution in matrix

The interaction between atoms can change the forces applying on the impurity, thus is an important factor affecting the migration behaviors. Fig. 3 illustrates the change in bond lengths by a substitutional impurity. It can be seen that both Cs and I exert a repulsive effect on the surrounding Cr atoms, because the Bader radii of Cs and I shown in Table 1 are both larger than that of Cr. The effect of Cs is more significant, with the bond lengths of its 1nn and 2nn increasing both by more than 0.1 Å.

To better understand the effect of impurities, the electronic structure with impurities was further analyzed. Using the Bader decomposition method [49], Bader charge, volume and radius [50] were listed in Table 1. For the Cr atoms, it is found that the Bader charge and atomic volume of the 127 Cr atoms are almost the same, so their average values are given directly in the table. It is observed that both Cs and I gain electrons from the matrix. In addition, the non-metallic I atom gains reasonably more electrons than the metallic Cs atom. The atomic volumes of Cs and I are almost the same when they occupy a substitutional site in Cr matrix, so it can be expected that there should be similarities in their migration behaviors.

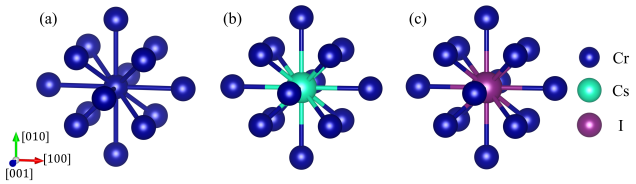

Bond length /Å	(a)	(b)	(c)
1nn	2.456	2.581	2.560
2nn	2.836	2.959	2.898

Fig. 3. (Color online) Calculated bond lengths (Å) in the Cr matrix for (a) pure matrix, (b) matrix with a substitutional Cs atom, (c) matrix with a substitutional I atom.

TABLE 1. Calculated Bader charge,volume and radius of atoms in Cr matrix with Cs or I substitution. Cr(Cs) denotes the Cr atom in Cs-doped Cr matrix, and Cr(I) means that in I-doped one.

	Cs	Cr(Cs)	I	Cr(I)
Bader charge/e^-	9.369	5.997	7.784	5.994
Atomic volume/Å^3	18.778	11.346	19.056	11.344
Atomic radius/Å	1.649	1.394	1.657	1.394

The binding effect between impurity atoms and their surrounding Cr atoms is weaker compared to that between Cr atoms, which can be observed from the charge densities between the impurity atoms and their 1nn Cr atoms shown in Fig. 4. It can be seen that the charge density around the impurity atoms decreases significantly compared to the corresponding profile for the pure Cr system (Fig. 4(a)), which is in agreement with the effect of increasing bond length in Fig. 3. Besides, the presence of the impurity atoms also increases the charge density between the Cr atoms in the diagonal direction, indicating an enhanced interaction between them. Taken together, the Cr atoms near the impurity atoms tend to move away from the impurity atoms and have a weak binding interaction with the impurity atoms, favoring the diffusion of the impurity atoms in the matrix.

In addition, the binding effect of Cr atoms to Cs is slightly weaker than that to I. Comparing the results of Cs and I (Fig. 4(b) & (c)), the charge density distributions are similar, but in terms of equipotential lines, the charge density around Cs is more dilute and the interaction with Cr atoms is weaker than that of I. This is also consistent with the fact that the Cs-Cr bonds are longer than the I-Cr bonds in Fig. 3, and can also be observed in Fig. 5. There is no hybridization peak between Cs and Cr atoms, indicating the metallic bonds; several hybridization peaks appear between I and Cr atoms, indicating covalent-like type bonds. Specifically, the d electrons of

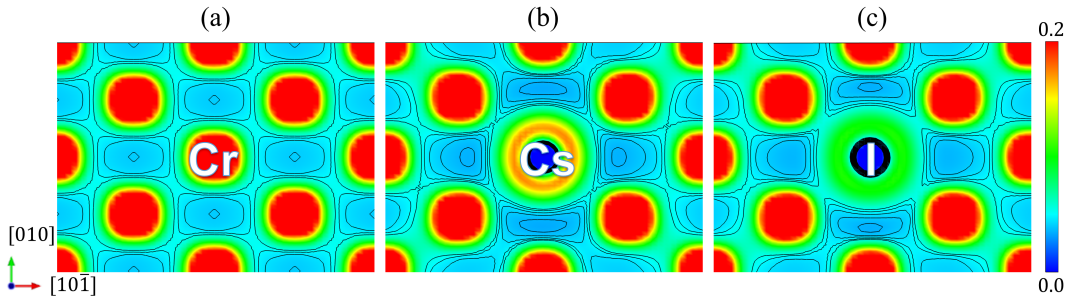

Fig. 4. (Color online) Calculated charge density distribution (electron/Bohr^3) in the (101) plane for (a) pure Cr matrix, (b) Cr matrix with a substitutional Cs atom, (c) Cr matrix with a substitutional I atom.

Cr and the p electrons of I are mainly involved in hybridization between -9 and -3 eV, and the d electrons of Cr and I are mainly involved in hybridization between -2 and 0 eV. Overall, Cs and I have similar effects on the Cr matrix, with slightly lower interactions around Cs than I.

2. Diffusion process and diffusion coefficient in matrix

In order to investigate the effect of impurity atoms on neighboring vacancies, the binding energies of impurity atoms to neighboring vacancies were calculated according to Eq.(6) and the results from 1nn to 4nn are shown in Fig. 6. The binding energy involved the 5nn vacancy is not presented, because the 5nn vacancy slides spontaneously into the 1nn position, i.e., the Cr atom in the 1nn position of the impurity slides spontaneously into the 5nn position. Both impurity atoms have an attractive effect on the vacancies from 1nn to 4nn. The binding energy of Cs to the 1nn vacancy is up to 2.46 eV, which is a possible reason for the formation of "V/2 + Cs + V/2" configuration. The relatively low binding energy between I and its 1nn vacancy may be the reason why I remains stable at the substitution site. The binding energies of Cs atom to vacancies are generally higher than those of I atom, especially for the 1nn and 2nn vacancies. But for the 3nn and 4nn vacancy, the binding energies are almost the same, indicating that the impurity atoms mainly affect the 1nn and 2nn vacancies.

Migration energy and the attempt frequency required for the vacancies near the impurity to move onto different sites are also important factors affecting the difficulty of migration processes. The results in Table 2 indicate that the impurity atoms are favored in the competition for vacancies with the surrounding matrix atoms. The migration barrier of vacancies moving away from the impurity atoms (E_3^m, $E_{3'}^m$, E_5^m) are generally higher than those in the direction close to the impurity atoms (E_4^m, $E_{4'}^m$, E_6^m), and the energy required for the vacancies located in the 3nn of the impurity atoms to migrate to the 1nn is lower than that required for self-diffusion in the pure Cr system (0.92 eV shown in Fig. 7). In terms of the attempted frequency, the attempt frequencies of vacancies moving away from the impurity atoms (ν_3, $\nu_{3'}$, ν_5) are also generally lower than the attempt frequencies near the impurity atoms (ν_4, $\nu_{4'}$, ν_6). This indicates that vacancies are more likely to be attracted to stay near the impurity atoms, which is also consistent with the results we obtained in Fig. 6, and this attractive effect to vacancies facilitates the diffusion of impurity atoms.

TABLE 2. Vacancy migration energies and attempt frequencies for vacancies nearby the Cs or I atom.

	Cs	I
E_2^m	/	0.36
E_3^m	2.70	1.66
E_4^m	1.19	0.96
$E_{3'}^m$	2.66	1.77
$E_{4'}^m$	0.35	0.59
E_5^m	/	1.09
E_6^m	/	0.59
ν_2	/	2.85
ν_3	5.56	7.22
ν_4	12.80	10.12
$\nu_{3'}$	9.79	10.04
$\nu_{4'}$	12.95	15.12
ν_5	/	8.74
ν_6	/	12.63

Both Cs and I can diffuse easily in Cr matrix because of their low migration barriers. As illustrated in Fig. 7(a) & (b), Cs will spontaneously move from the substitutional site to the middle point of the two lattice sites, while I should overcome a migration barrier of 0.36 eV to move to another substitutional site. Although the migration of I is not spontaneous, the migration barrier is lower than that for Cr atoms (0.92 eV according to our calculations). As a result, the diffusion of Cs and I are both easier than the Cr self-diffusion. Nevertheless, the results of migration barriers do not necessarily imply that Cs diffusion is faster than I, as the displacement of I that occurs by diffusion is $\sqrt{3}a/2$, which is twice of the displacement of Cs.

Before determination of the diffusion coefficients of Cs

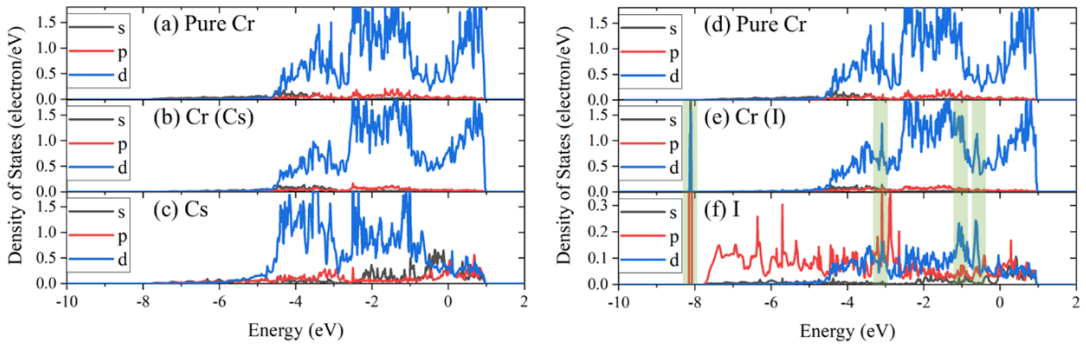

Fig. 5. (Color online) Density of states (DOS) with respect to the energy: (a)&(d) Cr in pure Cr matrix, (b)&(e) 1nn-Cr of a substitutional Cs or I atom, and (c)&(f) substitutional Cs and I atoms, respectively. Main hybridization peaks are marked with light green bars.

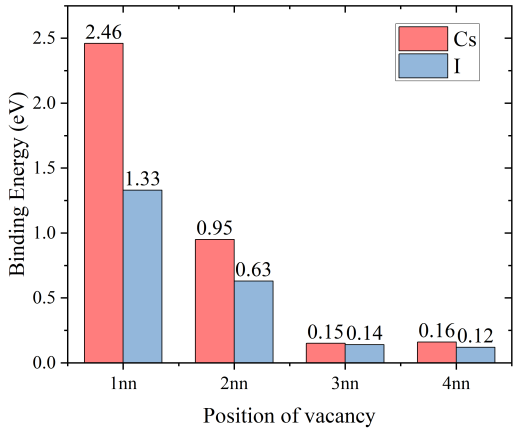

Fig. 6. (Color online) Calculated impurity-vacancy binding energies.

and I in Cr, approximations should be made for the phenomenon of spontaneous sliding of the 5nn vacancy of the impurity to the 1nn position. Since this process proceeds spontaneously, it is not possible to find the corresponding vacancy jump frequency according to Eq. (4). According to the assumptions of the Le Claire and OSA models, the frequency of the exchange of the 5nn vacancy with the atom further away from the impurity is considered to be the jump frequency of the Cr atom self-diffusion. In our DFT simulations, the 5nn vacancy will only slide into the 1nn position, so we can define:

$$\omega_{4''} = \omega_0, \quad \omega_{3''} = 0. \tag{8}$$

Based on all the assumptions made before, the diffusion coefficients of Cs and I in Cr matrix at 500 - 2000 K can be calculated according to OSA model and Le Claire model, respectively, as shown in Fig. 8. The results of Cr self-diffusion coefficients are shown for comparison, which are in good agreement with the experimental data [51, 52]. It can be seen that the diffusion coefficients of the impurity atoms are larger than the self-diffusion coefficients of Cr in the temperature interval considered. This can be attributed to the combined effect of the three factors analyzed in preceding paragraphs: weaker bonding effect by the surrounding Cr atoms, stronger attraction effect for nearby vacancies and lower migration barriers compared to the Cr self-diffusion process. In the temperature range of Generation IV fast reactors around 500 - 1000 K, the diffusion coefficients of Cs and I are 3 - 7 orders of magnitude larger than the self-diffusion coefficients of Cr, which also indicates the strong penetration ability of Cs and I. The diffusion coefficients of all the three elements increase exponentially with the increasing temperature. Despite the different diffusion characteristics of Cs and I shown in Fig. 7, the diffusion coefficients of Cs and I are very close at the temperature range considered. Because our calculations of Cr self-diffusion coefficients agree well with the experimental results, the diffusion coefficients of Cs and I in BCC Cr from DFT calculations are reliable.

The self-diffusion coefficient of BCC Cr, D_{Cr} (cm^2/s), can be recalculated using the follow equation based on parameters obtained in this study:

$$D_{Cr} = 0.1323 \times exp(-\frac{4.0861 \times 10^4}{T}), \tag{9}$$

and the diffusion coefficient of Cs and I in BCC Cr, D_{Cs} and D_I (cm^2/s), can be fitted from Fig. 8 as below:

$$D_{Cs} = exp[(-5.8676 \pm 0.0051) - \frac{(2.6915 \pm 0.0004) \times 10^4}{T}], \tag{10}$$

$$D_I = exp[(-1.8582 \pm 0.0158) - \frac{(3.4297 \pm 0.0016) \times 10^4}{T}]. \tag{11}$$

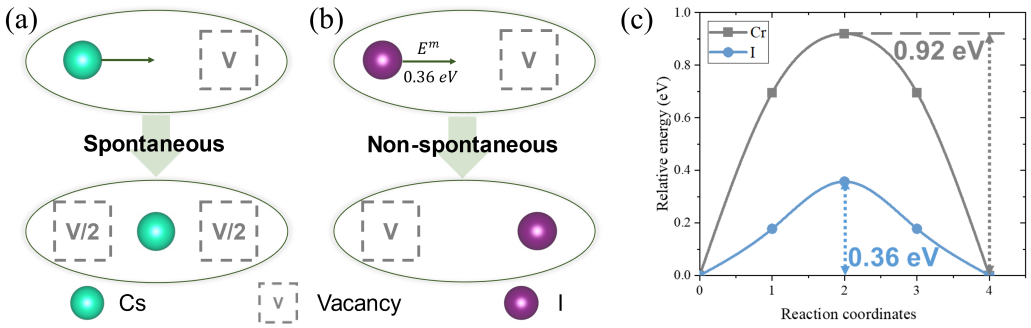

Fig. 7. (Color online) Illustration of diffusion characteristics of Cs and I. (a) Spontaneous diffusion of Cs; (b) Non-spontaneous diffusion of I; (c) Migration barriers of I and Cr. Energies are relative to the corresponding initial states.

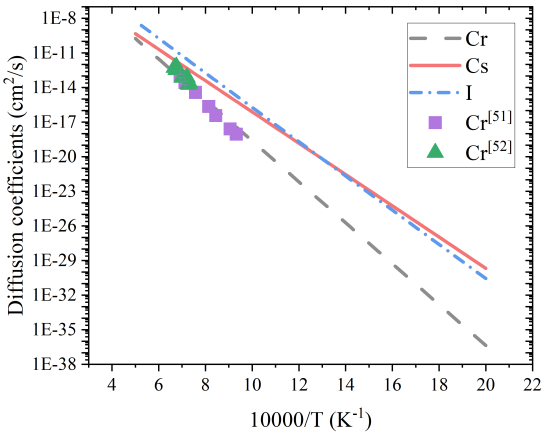

Fig. 8. (Color online) Temperature dependence of impurity diffusion coefficient in Cr matrix. Self-diffusion coefficients are given for comparison. Our results are denoted by lines and experimental results are denoted by dots.

B. Impurity diffusion at Cr GB

1. Atomic structure and electron distribution at the GB

GB serves as a fast diffusion channel for the impurity atoms, and the existence of Cs and I atoms on the GB plane will change the GB structures, such as bond lengths and charge distributions. In this subsection, the impurity atom was placed at site 1 on the GB plane to analyze the changes and the differences between matrix and GB. As shown in Fig. 9, the presence of impurity atoms at GB does not lead to the increase of all bond lengths, which is different from that in matrix. Nevertheless, the impurity atoms located at this substitution site significantly increase the bond length in the [210] direction, i.e., distancing the atoms on both sides of the GB plane. This facilitates the diffusion of the impurity atoms along the interface. Besides, Cs have a more pronounced effect on increasing this bond length than I, which is in accord with the results in Fig. 3.

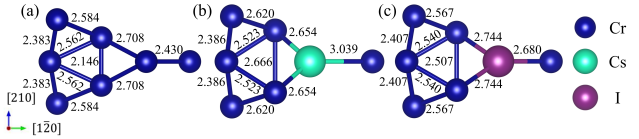

Fig. 9. (Color online) Calculated bond lengths (Å) at Cr GB for (a) pure GB, (b) GB with a substitutional Cs atom, (c) GB with a substitutional I atom.

TABLE 3. Calculated Bader charge,volume and radius of atoms at Cr GB. The values of Cr are averaging values. Cr (Cs) denotes the Cr atom in Cs-doped Cr GB, and Cr (I) means that in I-doped one.

	Cs	Cr(Cs)	I	Cr(I)
Bader charge/e^-	8.962	6.001	7.600	5.992
Atomic volume/Å^3	21.286	11.881	21.968	11.872
Atomic radius/Å	1.719	1.416	1.737	1.415

The Bader charge, volume and radius [50] of atoms at GB were obtained using the Bader decomposition method [49] as in matrix, and the results are demonstrated in Table 3. As in the matrix, the Bader results of the 75 Cr atoms at GB were found close, so their average values were used for analysis. Comparing Table 1 with Table 3, it is found that the I atom gains electrons both in matrix and at GB, while the Cs atom loses electrons at GB, which is different from the case in matrix. For I substitution, the number of electrons gained at the GB is slightly less compared to that in the matrix, probably because the atomic structure at GB is not as compact as in the matrix and the electrons are transferred less between the different nuclei. The atomic volumes of Cs and I at Cr GB are essentially the same as in Cr matrix. The difference is that the Bader volume of all atoms at GB is slightly larger than that in matrix, which is reasonable because the atomic arrangement at GB is sparser. This

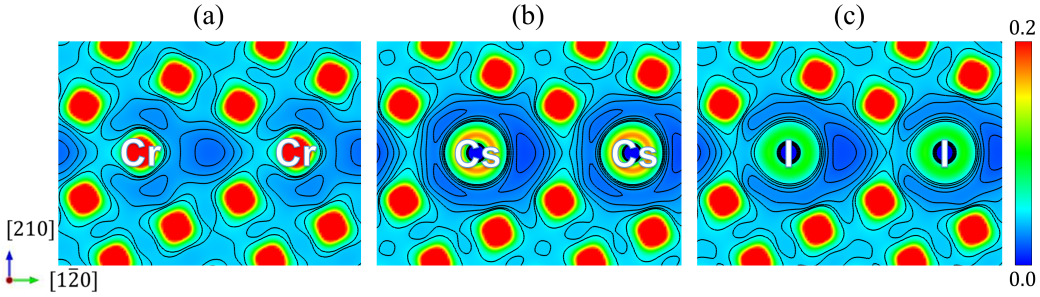

Fig. 10. (Color online) Calculated charge density distribution (electron/Bohr^3) in the (001) plane for (a) pure GB, and GB with a substitutional (b) Cs or (c) I atom at site 1.

is also favorable to the migration of Cs and I atoms, and it can be expected that the impurity atoms on the GB plane will migrate more easily than in matrix.

Both Cs and I have similar effects at Cr GB as in matrix, with slightly lower interactions around Cs than I, as shown in the distribution of charge densities in Fig. 10. It can be seen that the charge density around the impurity atoms is significantly lower compared to that at pure Cr GB, which is similar as in Cr matrix (Fig. 4). The dilute charge density indicates a weak interaction between the impurity atoms with their surrounding Cr atoms, which favors the migration of the impurity atoms along the GB plane. Comparing the charge distributions in Fig. 10(b) & (c), it can be seen that the charge density around Cs is smaller than that around I, i.e. the Cs-Cr binding is weaker than the I-Cr one, which also agree with the change in the bond length in [210] direction in Fig. 9. Compared to the charge density distribution in the matrix (Fig. 4), the charge density distribution at GB is more dilute. As a result, it can be predicted that the diffusion rates of Cs and I at GB should be comparable, and the diffusion should be much easier than in matrix.

2. Diffusion barrier and diffusion path along the GB

To investigate the impurity diffusion behaviors along GB, impurity atoms were placed at interstitial site 0, substitutional sites 1 and 2 on the GB plane (as shown in Fig. 2(b)) respectively as initial structures of different migration processes, and the results of the optimization of these initial structures are shown in Table 4. It can be observed that the impurity atoms located in site 0 will spontaneously migrate to the non-occupied site 2, which is more stable than site 0. If a vacancy is introduced at site 1, the impurity atoms located at site 2 will spontaneously migrate to site 1, which is more stable than site 2. Both of these migration processes take place spontaneously, so that the impurity atoms can readily diffuse along the GB direction.

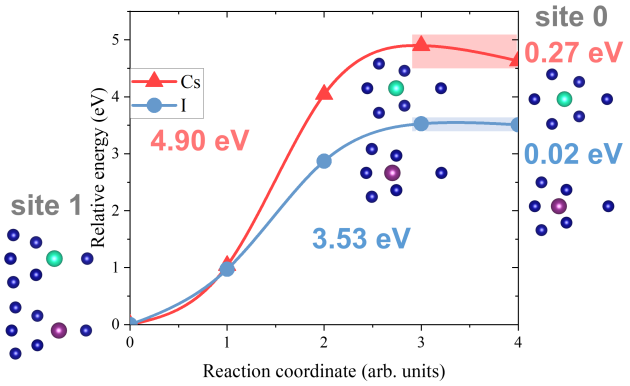

Fig. 11. (Color online) Evaluation of energy during the Cs or I migration process between sites 0 and 1 at GB. Energies are with respect to the initial structure with impurity atom at site 1.

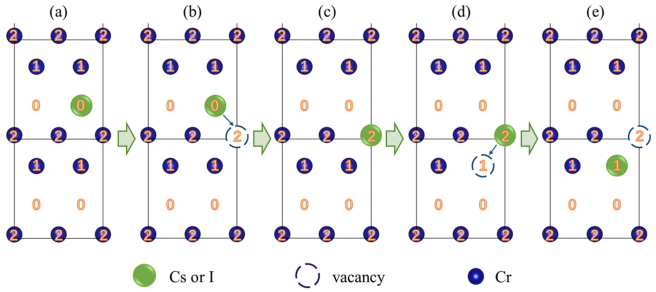

Fig. 12. (Color online) First-principles predicted paths of spontaneous impurity diffusion along GB plane: (a) impurity atoms initially located at site 0; (b) introduction of a vacancy at site 2; (c) spontaneous movement of impurity atoms to site 2; (d) introduction of a vacancy at site 1; (e) spontaneous movement of impurity atoms to site 1.

The calculated migration barriers between site 0 and site 1 are shown in Fig. 11. The migration barriers from

TABLE 4. Atomic structures after ionic optimization by first-principles calculation.

Migration process	Initial structure (vacancy site, impurity site)	Final position of Cs after optimization	Final position of I after optimization
site 2 → site 0	(site 0, site 2)	site 2	site 2
site 0 → site 2	(site 2, site 0)	Between site 0 and site 2	site 2
site 1 → site 2	(site 2, site 1)	Between site 1 and site 2, closer to site 1	site 1
site 2→ site 1	(site 1, site 2)	Between site 1 and site 2, closer to site 1	site 1
site 1 → site 0	(site 0, site 1)	site 1	site 1
site 0 → site 1	(site 1, site 0)	site 0	site 0

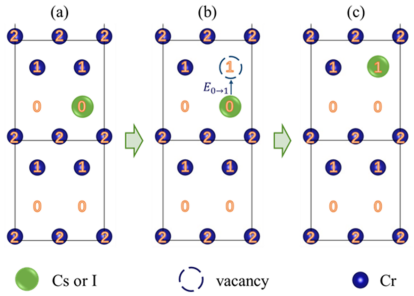

Fig. 13. (Color online) First-principles predicted diffusion paths of impurity atoms along GB plane by overcoming a low migration barrier: (a) impurity atoms initially located at site 0; (b) introduction of a vacancy at site 1; (c) impurity atoms diffusion to site 1 with a low energy barrier.

site 0 to site 1 for Cs and I are obviously smaller compared to those in matrix (Table 2), indicating that GBs are fast channels for the impurity diffusion in Cr. Nevertheless, it can be seen that Cs or I needs to overcome a high energy barrier (up to 4.90 eV or 3.53 eV) to migrate from site 1 to site 0, meaning that impurity diffusion is directional in some GB regions.

In summary, two more possible paths were predicted for the diffusion of impurity atoms along GB plane, as shown in Fig. 12 & 13. Both migration paths require the introduction of vacancies at the GB plane, and lots of vacancies exist at the GB region of real materials. Furthermore, the vacancy concentration can be significantly increased by the combined effect of high temperature and irradiation under service conditions on the inner surface of the cladding in nuclear reactor. In Fig. 12, vacancies at sites 2 and 1 were introduced in succession, and the impurity atoms at site 0 move spontaneously, sliding sequentially to site 2 and then to site 1. In Fig. 13, one vacancy was introduced at site 1, and due to the low migration barrier from sites 0 to 1, the impurity atoms can easily move to site 1.

IV. SUMMARY

Diffusion behaviors of Cs and I, key elements of FCCI, in Cr coating were investigated using DFT approaches together with Le Claire and OSA diffusion models. Under the combined effect of low binding effect with matrix atoms and strong binding effect with nearby vacancies, the migration barriers of Cs and I are both lower compared to that of Cr. As a result, the diffusion coefficients of Cs and I are both 3-7 order of magnitude larger than that of Cr's self-diffusion coefficient below 1000 K, which corresponds to the temperature range of Generation IV fast reactors. Despite the difference of migration barriers and displacements of the elemental diffusion process of Cs and I, and also the different models used, the diffusion coefficients obtained for Cs and I are basically the same order of magnitude at temperature considered. Meanwhile, the results of Cr self-diffusion agree well with experimental values, judged by which our results can be considered accurate. Based on our results, the diffusion paths of Cs and I in the inner-surface Cr coating of the cladding were predicted. Cs and I are more likely to diffuse along the GB, and the intergranular corrosion still requires for further investigations.

V. APPENDIX

TABLE 5. List of abbreviation.

Abbreviation	Definition
BCC	Body Centered Cubic
cNEB	climbing image Nudged Elastic Band
DFT	Density Functional Theory
FCCI	Fuel Cladding Chemical Interaction
GB	Grain Boundary
nn	nearest neighbors
OSA	Oversized Solute-Atom
PAW	Projector Augmented Wave
PBE	Perdew-Burke-Ernzerhof
VASP	Vienna ab initio simulation package

[1] K. Maeda, 3.16 - Ceramic Fuel–Cladding Interaction, in: R.J.M. Konings (Ed.) Comprehensive Nuclear Materials, Elsevier, Oxford, 2012, pp. 443-483.

[2] R. Parrish, A. Aitkaliyeva, A review of microstructural features in fast reactor mixed oxide fuels. J. Nucl. Mater. 510, 644-660 (2018). doi:10.1016/j.jnucmat.2018.05.076

[3] W. Zhong, P.A. Mouche, B.J. Heuser, Response of Cr and Cr-Al coatings on Zircaloy-2 to high temperature steam. J. Nucl. Mater. 498, 137-148 (2018). doi:10.1016/j.jnucmat.2017.10.021

[4] J.-C. Brachet, I. Idarraga-Trujillo, M.L. Flem et al., Early studies on Cr-Coated Zircaloy-4 as enhanced accident tolerant nuclear fuel claddings for light water reactors. J. Nucl. Mater. 517, 268-285 (2019). doi:10.1016/j.jnucmat.2019.02.018

[5] J. Jiang, H. Zhai, P. Gong et al., In-situ study on the tensile behavior of Cr-coated zircaloy for accident tolerant fuel claddings. Surf. Coat. Technol. 394, 125747 (2020). doi:10.1016/j.surfcoat.2020.125747

[6] J. Jiang, D. Zhan, J. Lv et al., Comparative study on the tensile cracking behavior of CrN and Cr coatings for accident-tolerant fuel claddings. Surf. Coat. Technol. 409, 126812 (2021). doi:10.1016/j.surfcoat.2020.126812

[7] J.-S. Jiang, D.-Q. Wang, M.-Y. Du et al., Interdiffusion behavior between Cr and Zr and its effect on the microcracking behavior in the Cr-coated Zr-4 alloy. Nucl. Sci. Tech. 32, 134 (2021). doi:10.1007/s41365-021-00977-w

[8] J. Bischoff, C. Delafoy, N. Chaari et al., Cr-coated cladding development at Framatome, Topfuel 2018-Light Water Reactor (LWR) Fuel Performance Meeting 2018, 2018.

[9] J. Bischoff, C. Delafoy, C. Vauglin et al., AREVA NP's enhanced accident-tolerant fuel developments: Focus on Cr-coated M5 cladding. Nucl. Eng. Technol. 50, 223-228 (2018). doi:10.1016/j.net.2017.12.004

[10] J. Yang, M. Steinbrück, C. Tang et al., Review on chromium coated zirconium alloy accident tolerant fuel cladding. J. Alloys Compd. 895, 162450 (2022). doi:10.1016/j.jallcom.2021.162450

[11] H. Wu, T. Mayeshiba, D. Morgan, High-throughput ab-initio dilute solute diffusion database. Sci. Data 3, (2016). doi:10.1038/sdata.2016.54

[12] C.E. Campbell, W.J. Boettinger, U.R. Kattner, Development of a diffusion mobility database for Ni-base superalloys. Acta Mater. 50, 775-792 (2002). doi:10.1016/S1359-6454(01)00383-4

[13] A. Janotti, M. Krčmar, C. Fu et al., Solute diffusion in metals: larger atoms can move faster. Phys. Rev. Lett. 92, 085901 (2004). doi:10.1103/PhysRevLett.92.085901

[14] M. Krčmar, C.L. Fu, A. Janotti et al., Diffusion rates of 3d transition metal solutes in nickel by first-principles calculations. Acta Mater. 53, 2369-2376 (2005). doi:10.1016/j.actamat.2005.01.044

[15] I. Lomaev, D. Novikov, S. Okatov et al., First-principles study of 4d solute diffusion in nickel. J. Mater. Sci. 49, 4038-4044 (2014). doi:10.1007/s10853-014-8119-1

[16] W.-G. Liu, H. Han, C.-L. Ren et al., The effect of Nb additive on Te-induced stress corrosion cracking in Ni alloy: a first-principles calculation. Nucl. Sci. Tech. 25, 050603 (2014). doi:10.13538/j.1001-8042/nst.25.050603

[17] S. Huang, D.L. Worthington, M. Asta et al., Calculation of impurity diffusivities in -Fe using first-principles methods. Acta Mater. 58, 1982-1993 (2010). doi:10.1016/j.actamat.2009.11.041

[18] H. Ding, S. Huang, G. Ghosh et al., A computational study of impurity diffusivities for 5d transition metal solutes in -Fe. Scr. Mater. 67, 732-735 (2012). doi:10.1016/j.scriptamat.2012.06.010

[19] L. Messina, M. Nastar, T. Garnier et al., Exact ab initio transport coefficients in bcc Fe -X (X=Cr, Cu, Mn, Ni, P, Si) dilute alloys. Phys. Rev. B 90, 104203 (2014). doi:10.1103/PhysRevB.90.104203

[20] L. Messina, M. Nastar, N. Sandberg et al., Systematic electronic-structure investigation of substitutional impurity diffusion and flux coupling in bcc iron. Phys. Rev. B 93, 184302 (2016). doi:10.1103/PhysRevB.93.184302

[21] J.-L. Bocquet, C. Barouh, C.-C. Fu, Migration mechanism for oversized solutes in cubic lattices: The case of yttrium in iron. Phys. Rev. B 95, (2017). doi:10.1103/PhysRevB.95.214108

[22] C. Yang, J. Tian, H. Guan et al., Significant difference of lanthanide fission products diffusion in Cr and -Fe: An atomic-level study. Scr. Mater. 227, 115304 (2023). doi:10.1016/j.scriptamat.2023.115304

[23] X. Gao, H. Ren, C. Li et al., First-principles calculations of rare earth (Y, La and Ce) diffusivities in bcc Fe. J. Alloys Compd. 663, 316-320 (2016). doi:10.1016/j.jallcom.2015.12.129

[24] D. Murali, B.K. Panigrahi, M.C. Valsakumar et al., Diffusion of Y and Ti/Zr in bcc iron: A first principles study. J. Nucl. Mater. 419, 208-212 (2011).doi:10.1016/j.jnucmat.2011.05.018

[25] N. Sandberg, R. Holmestad, First-principles calculations of impurity diffusion activation energies in Al. Phys. Rev. B 73, 014108 (2006). doi:10.1103/PhysRevB.73.014108

[26] M. Mantina, S. Shang, Y. Wang et al., 3 d transition metal impurities in aluminum: a first-principles study. Phys. Rev. B 80, 184111 (2009). doi:10.1103/PhysRevB.80.184111

[27] D. Simonovic, M.H. Sluiter, Impurity diffusion activation energies in Al from first principles. Phys. Rev. B 79, 054304 (2009). doi:10.1103/PhysRevB.79.054304

[28] J. Hui, B.-L. Zhang, T. Liu et al., Effects of impurity elements on SiC grain boundary stability and corrosion. Nucl. Sci. Tech. 32, 125 (2021). doi:10.1007/s41365-021-00963-2

[29] C. Wert, C. Zener, Interstitial Atomic Diffusion Coefficients. Phys. Rev. 76, 1169 (1949). doi:10.1103/PhysRev.76.1169

[30] Y. He, Y. Li, C. Chen et al., Diffusion coefficient of hydrogen interstitial atom in -Fe, -Fe and -Fe crystals by first-principle calculations. Int. J. Hydrog. Energy 42, 27438-27445 (2017). doi:10.1016/j.ijhydene.2017.08.212

[31] D. Connétable, M. David, Diffusion of interstitial species (H and O atoms) in fcc systems (Al, Cu, Co, Ni and Pd): Contribution of first and second order transition states. J. Alloys Compd. 772, 280-287 (2019). doi:10.1016/j.jallcom.2018.09.042

[32] M. David, A. Prillieux, D. Monceau et al., First-principles study of the insertion and diffusion of interstitial atoms (H, C, N and O) in nickel. J. Alloys Compd.

822, 153555 (2020). doi:10.1016/j.jallcom.2019.153555
[33] X. Yan, P. Li, L. Kang et al., First-principles study of electronic and diffusion properties of intrinsic defects in 4H-SiC. J. Appl. Phys. 127, 085702 (2020). doi:10.1063/1.5140692
[34] R. Abbaschian, R.E. Reed-Hill, Physical metallurgy principles-SI version, Cengage Learning2009.
[35] A. Le Claire, Solvent self-diffusion in dilute bcc solid solutions. Philos. Mag. 21, 819-832 (1970). doi:10.1080/14786437008238468
[36] M.J. Jones, A.D. Le Claire, Solvent self-diffusion in dilute b.c.c. solid solutions. Philos. Mag. 26, 1191-1204 (1972). doi:10.1080/14786437208227373
[37] A. Le Claire, Solute diffusion in dilute alloys. J. Nucl. Mater. 69, 70-96 (1978). doi:10.1016/0022-3115(78)90237-4
[38] G.H. Vineyard, Frequency factors and isotope effects in solid state rate processes. J. Phys. Chem. Solids 3, 121-127 (1957). doi:10.1016/0022-3697(57)90059-8
[39] G. Kresse, J. Hafner, Ab initio molecular dynamics for liquid metals. Phys. Rev. B 47, 558-561 (1993). doi:10.1103/physrevb.47.558
[40] G. Kresse, J. Furthmüller, Efficiency of ab-initio total energy calculations for metals and semiconductors using a plane-wave basis set. Comp. Mater. Sci. 6, 15-50 (1996). doi:10.1016/0927-0256(96)00008-0
[41] G. Kresse, J. Furthmüller, Efficient iterative schemes for ab initio total-energy calculations using a plane-wave basis set. Phys. Rev. B 54, 11169 (1996). doi:10.1103/PhysRevB.54.11169
[42] P.E. Blochl, Projector augmented-wave method. Phys. Rev. B. 50, 17953-17979 (1994). doi:10.1103/PhysRevB.50.17953
[43] J.P. Perdew, K. Burke, M. Ernzerhof, Generalized gradient approximation made simple. Phys. Rev. Lett. 77, 3865 (1996). doi:10.1103/PhysRevLett.77.3865
[44] V.I. Razumovskiy, A.V. Ruban, P.A. Korzhavyi, First-principles study of elastic properties of Cr- and Fe-rich Fe-Cr alloys. Phys. Rev. B 84, (2011). doi:10.1103/PhysRevB.84.024106
[45] G. Ho, M.T. Ong, K.J. Caspersen et al., Energetics and kinetics of vacancy diffusion and aggregation in shocked aluminium via orbital-free density functional theory. Phys Chem Chem Phys 9, 4951-4966 (2007). doi:10.1039/b705455f
[46] N. Zou, H.-J. Lu, X.-G. Lu, Impurity diffusion coefficients in BCC Nb from first-principles calculations. J. Alloys Compd. 803, 684-688 (2019). doi:10.1016/j.jallcom.2019.06.293
[47] X. Tang, R. Salehin, G.B. Thompson et al., Statistical study of vacancy diffusion in TiC and TaC. Phys. Rev. Mater. 4, (2020). doi:10.1103/PhysRevMaterials.4.093602
[48] L. Yang, N. Kaltsoyannis, Diffusion of krypton and xenon in uranium mononitride; a Density Functional Theory Study. J. Nucl. Mater. 566, 153803 (2022). doi:10.1016/j.jnucmat.2022.153803
[49] G. Henkelman, A. Arnaldsson, H. Jónsson, A fast and robust algorithm for Bader decomposition of charge density. Comp. Mater. Sci. 36, 354-360 (2006). doi:10.1016/j.commatsci.2005.04.010
[50] R.F. Bader, Atoms in molecules. Acc. Chem. Res. 18, 9-15 (1985). doi:10.1021/ar00109a003
[51] J.N. Mundy, C.W. Tse, W.D. McFall, Isotope effect in chromium self-diffusion. Phys. Rev. B 13, 2349-2357 (1976). doi:10.1103/PhysRevB.13.2349
[52] J.N. Mundy, H.A. Hoff, J. Pelleg et al., Self-diffusion in chromium. Phys. Rev. B 24, 658-665 (1981). doi:10.1103/PhysRevB.24.658